19

A CFD Study of Passive Solar Shading

[1]Baxevanou C.A.*, [1]Fidaros D.K., [2]Tzachanis A.D.
[1]*Centre for Research and Technology-Thessaly, Institute of Technology and Management of Agricultural Eco-systems, Technology Park of Thessaly, 1st Industrial Area of Volos, 38500 Volos, Greece, cbaxe@cereteth.gr, dfeid@cereteth.gr*
[2]*Technological Educational Institute (TEI) of Larissa, Dept. of Mechanical Engineering, 41110 Larissa, Greece, tzach@teilar.gr*

Abstract
In the present study is investigated numerically the flow and transport phenomena in a test cell with its south side partially shaded by trailing plants and the cover shaded by a shelter. The two dimensional unsteady transport equations for the velocities, turbulence, energy and spectral intensity of radiation are solved numerically by a finite volume numerical model. The turbulent nature of the flow is simulated by the well known two equation k-ω high Re model while the incident radiation is used the Discrete Ordinates (DO) model and two wavelength bands are considered for the solar and thermal radiation. The model efficiently renders the buoyancy effects inside the cell, the cooling capacity of the plants, the heat transfer phenomena of solar radiation and heat conduction through the cell walls. The thermophysical and spectral optical properties of the involved materials were taken into account and not only the shading effect of trailing plant. The model was validated successfully via comparison with measured data that correspond in one day of August in Central Greece. A parametric study was carried out for other 4 months (May, June, July and September). The results are given in terms of fields of flow, radiation and temperature inside the test cell and in the space between this and the shading devices (shelter and trailing plants). Daily variations of average temperatures, solar radiation, air flow velocities and cooling load reduction are also given. The cooling load reduction ranges between 34 kWh/month per wall meter in September, and 63 kWh/month per wall meter in July, even without taking into account the temperature reduction due to the plants transpiration. The developed model can be used for the evaluation of various plants performance as passive solar shading configurations.

Notation

a	porous permeability [m^2]
C_2	inertial resistance factor [1/m]
C_p	specific heat capacity [J/(kg K)]
d	thickness [m]
e	specific energy (per unit mass) [J/Kg]

f_b	buoyancy force [Nt/m^3]
f_d	diffuse fraction of incident radiation [-]
h	sensible enthalpy [J/Kg], convective heat transfer coefficient [W/m^{2}K]
G	normal solar irradiation [W/m^2]
$\overline{H_b}$	monthly average daily beam irradiation [Wh/m^2]
$\overline{H_d}$	monthly average daily diffuse radiation [Wh/m^2]
$\overline{H_{tot}}$	the monthly average daily radiation [Wh/m^2]
I	radiation intensity [W/m^2]
I_v	radiation intensity normal to vertical plane [W/m^2]
I_h	radiation intensity normal to horizontal plane [W/m^2]
I_λ	radiation intensity for wavelength λ [W/(m^2 src)]
$I_{b\lambda}$	black body intensity given by the Planck function [W/m^2]
k	turbulent kinetic energy [J/Kg], Thermal conductivity [W/mK]
k_{eff}	effective conductivity [W/mK]
k_t	turbulent thermal conductivity [W/mK]
L	latitude [deg]
n	refractive index of medium b [-], number of the day of a year [-]
NT	total daily duration of sunlight [h]
Nu	nusselt number [-] (Nu=convection/conduction) Nu=hL/K
P	pressure [Pa]
r_i	reflectivity of medium I [-]
$\vec{r}$	position vector [-]
R_b	the ratio of beam irradiation on the plane to that on a horizontal plane [-]
S_h	radiation source term [J]
$\vec{s}$	radiation direction vector [-]
t	time [s]
time	time since sunrise [sec]
t_s	sunrise time [h]
T	temperature [K]
Ta	ambient temperature [K]
T_0	operating reference temperature [K]
U_i	average velocity in i-direction [m/s]
x_i	component in i-direction [m]

Greek Letters

α	absorptivity [-]
α_λ	spectral absorption coefficient [1/m] – or extinction coefficient
β	Thermal expansion coefficient [1/K], the surface slope [deg]
γ	the surface azimuth angle [deg]
δ	declination [deg]
ε	turbulent dissipation rate [J/(Kg s)], emissivity [-]
θ_a	angle between the normal to the surface and the incident radiation [deg]
θ_b	angle between the normal to the surface and the refracted radiation [deg]
θ_z	solar zenith angle [deg]

λ wavelength [m^{-1}]
μ viscosity [Pa sec]
μ_t turbulent viscosity [Pa sec]
ρ density [kg/m^3]
ρ_0 constant flow density [kg/m^3]
σ_s scattering coefficient [1/m]
$(\tau_{ij})_{eff}$ effective stress tensor [Nt/m^2]
τ_i transmissivity of medium i [-]
Φ phase function [-]
ω specific dissipation rate [s^{-1}] , hour angle [deg]
ω_s sunrise hour angle [deg]
Ω' solid angle [deg]

1. Introduction

The placing of plants in the vicinity of the south walls of a building as solar protection system is an old and well-known technique in traditional architecture and a basic parameter in bioclimatic design, especially for countries with a climate characterized by long hot days in the summers. Plants offer the potential of solar control in buildings as well as of passive cooling. Deciduous plants can reduce excessive solar heat gains during the summer allowing the solar light to reach the building's interior during the summer. This way they contribute in reduction of air conditioning devices usage during the periods of peak power demand (Achard, P. & Gicquel, R., 1986; Goulding, J. R. et al., 1993). It has been proved that by adding one tree the cooling energy savings can vary in the range of 12-24%. Three trees per house could reduce the cooling load from 17% to 57% (Akbari, H. et al., 1997; Raeissi, S. & Taheri, M., 1999). Plants can achieve this reduction operating in two ways: a) operating as natural shading and b) reducing the air temperature through transpiration. Plants not only improve the building's energy performance during summer but they also affect appearance of them as they can be incorporated in the architectural design offering an acceptable and aesthetical result (Carter, C. & De Villiers, J., 1987; Goulding, J. R. et al., 1992).
In the present study a numerical model is developed in order to study the transport phenomena in a test cell with its south façade partially shaded by trailing deciduous plant called *Parthenocissus quinquefoliant*. It is taken into account the plants' shading effect taking account their optical properties and their ability of heating storage but not the transpiration. The numerical model will be validated against existed measurements. Then a parametric numerical study will allow the systematic quantification of the energy gains which could establish a new way of thinking for passive cooling design.

2. Literature review

Until now the majority of studies about plants as passive solar devices, concerned the experimental investigation of the energy saving and alteration of the building internal microclimate offered by the plants' shadow.
According to measurements in two houses (Akbari, H., Kurn, D. M. et al., 1997) the cooling energy saving yielded by trees appearance can reach levels up to 30% corresponding to daily savings of 3.6 to 4.8 kWh/d. Experimental investigation of shading with trees,

positioned around buildings - especially on the southern side (Papadakis, G. et al., 2001) have also been performed. The results have shown that trees constitute an excellent passive cooling system, being able to reduce the peak solar heat gain from 600 W/m^2 to 180 W/m^2, even with measured temperatures in the sunlit and in the shaded area of about 42^{o}C and 33^{o}C respectively.
Another group of studies developed analytical models which usually have been incorporated in software. In the paper (Tzachanis, A. D. & Sdravopoulou, C., 2002) the periodic steady heat gain in buildings is simulated with a dynamic model. In the work (Liu, Y. & Harris, D. J., 2008) an energy software package, the ESP-r, was used in order to study the effect of trees sited in the north of a house, in the heating-energy consumption.
Recently numerical methods are used for the study of heat transfer mainly in solar chimneys (Gan, G., 2006; Miyazaki, T. et al., 2006) used in the south facades. Numerical methods are more widely used for study of the microclimate developed in urban street canyons (Erell, E. & T. Williamson, 2006; Ali-Toudert, F. & Mayer, H., 2007).
As far it concerns numerical studies for the use of plants as passive solar systems there are some hybrid approaches like the one presented in (Mochida, A. et al., 2006) where a CFD model is used for the study of convective and radiative heat transports phenomena around buildings and the program 'TRNSYS' for the heat load calculations inside them.
In the numerical study (Baxevanou, C. A. et al., 2008) the test cell of present study was investigated considering the plants only as a shading device without taking into account exact optical and thermal properties and the temporal heat storage. Nevertheless this preliminary work was the starting point for the numerical model presented here.

3. Physical problem

In the present study the flow and transport phenomena inside and around a test cell with its south side shaded by trailing plant is investigated numerically. The physical model is an experimental setup of a cubic shaped test cell having a volume of approximately 30m^3 build at the TEI of Larissa, Greece (Tzachanis, A. D., 2008). This set-up gives the possibility to carry out experiments "in situ" with the instrumentation and the data acquisition system being placed inside the cell and is presented in Fig.1. Its south face is shaded by trailing plant called *Parthenocissus quinquefoliant*. The test cell walls are fabricated by a 5 cm sandwich material consisting of a 4.8 cm polyurethane layer with steel claddings. The whole construction was placed on a steel frame with wheels enabling easily the orientation change of the cell. Over the ceiling there is an inclined shelter of the same material that allows the cell cooling by convection from the air circulating between the ceiling and the shelter.

Fig. 1. A front view of the passive solar system

3.1 Geometry

In the following Fig.2 the geometry of a test cell cross-section is presented.

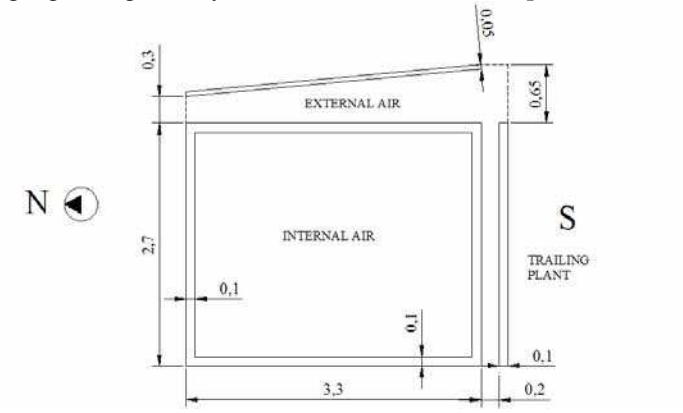

Fig. 2. Cross-section geometry

3.2 Properties

In the following tables the thermophysical and spectral optical properties of the involved materials are given. As it is said the walls are sandwich of polyurethane and steel cladding painted white. In this simulation is considered as a homogenous material with the effective properties given in the following Table 1. The plants' optical properties correspond to

tomato crop according to (Zhang, Y. et al., 1997) and they are radiation wave length depended. They are given for two spectral bands, the first is considered as solar band and corresponds to wavelength λ=0-1.1 μm and the second is considered as thermal band and corresponds to wavelength λ=1.1–100 μm. The trailing plants are modelled as porous medium where the 40% of the total volume is air. The air is considered to contain enough vapors to present noticeable absorptivity (Modest, M. F., 2003).

Property	Air	Plant		Walls
		λ=0-1.1	λ=1.1-100	
Density, ρ [Kg/m³]	1.225	700		807
Specific Heat Capacity, Cp, [J/KgK]	1006.43	2310		465
Conductivity, k [W/m]	0.0242	0.173		0.0255
Viscosity, μ [Pasec]	1.789×10^{-5}	-		-
Thermal expansion coefficient, β [1/K]	0.00343	-		-
Absorptivity, α	0.19	0.71	0.95	0.85
Refractive index, n	1	2.69	1.22	24.62
Emissivity, ε	0.05	0.59		0.45
Transmissivity, τ	0.81	0.08	0	0

Table 1. Material properties

4. Mathematical model

In this work we study the flow and the transport phenomena developed in the air inside the test cell, the air between the test cell and the shading devices (shelter and trailing plants) and the solid materials involved (test cell walls, shelter and trailing plants). The flow is assumed to be 2D, incompressible, unsteady and turbulent since those phenomena are studied along the symmetry cross-section in the North-South plane as shown in Fig.2. This simplification is adopted in this study in order to save computational effort although the aspect ratio of the sides is rather small. The flow and transport phenomena for air flow and heat and radiation transfer are described by the Navier-Stokes equations (Ferziger, J. H. & Perić, M., 2002).

4.1 Transport equations

The time-averaged Navier-Stokes equations, for the mass and momentum transport are given as follow (Launder, B. E. & Spalding, D. B., 1974):

Continuity equation

$$\frac{\partial U_i}{\partial x_i} = 0 \tag{1}$$

Momentum conservation

$$\rho\left(\frac{\partial U_i}{\partial t} + U_j \frac{\partial U_i}{x_j}\right) = -\frac{\partial P}{\partial x_j} + \frac{\partial}{\partial x_j}\left[\left(\mu + \mu_t\right)\frac{\partial U_i}{\partial x_j}\right] + f_b + S_i \tag{2}$$

Where, U_i the time averaged i-direction velocity, ρ the density, P the pressure, μ the viscosity, μ_t the turbulent viscosity, f_b the buoyancy force, t the time and S_i source term

expressing the pressure drop across the plants which are considered to be porous medium.

4.2. Boussinesq approximation

The density variation is calculated according to the Boussinesq model in order to take into account the natural convection effects. The use of Boussinesq model offers faster convergence, than considering the density variable in all equations. In this model the density is a constant value in all solved equations except from the buoyancy term calculation in the momentum equation:

$$f_b = (\rho - \rho_0) g \approx -\rho_0 \beta (T - T_0) g \tag{3}$$

This way the ρ is eliminated from the buoyancy term using the Boussinesq approximation:

$$\rho = \rho_0 (1 - \beta \Delta T) \tag{4}$$

Where β is the thermal expansion coefficient, T the temperature, ρ_o and T_o the corresponding reference values for density and temperature and g the gravity acceleration.

4.3 Porous media Treatment

The trailing plants, which are a shading device, are simulated as porous media adding a momentum source term S_i to the Navier-Stokes fluid flow equation. This term express the pressure drop caused in the flow by their presence and it is composed by a viscous loss term known as Darcy law and an inertial loss term, according to the following:

$$S_i = -\left(\frac{\mu}{\alpha} u_i + C_2 \rho u_i^2 \right) \tag{5}$$

where, a is the porous permeability and C_2 the inertial resistance factor.

4.4 Energy Treatment

Energy Conservation is described by the following equation

$$\rho \left(\frac{\partial h}{\partial t} + U_i \frac{\partial h}{\partial x_i} \right) = k_{eff} \frac{\partial}{\partial x_i} \left(\frac{\partial T}{\partial x_i} \right) + S_h \tag{6}$$

Where ε is specific energy (per unit mass), k_{eff} the effective conductivity, $(\tau_{ij})_{eff}$ the effective stress tensor and S_h source term which add the radiation contribution to the energy conservation equation. Auxiliary relationships for the calculations of quantities appeared in energy equation are presented here. Specifically relationships are given for the calculation of effective and turbulent conductivity as well as for the energy and enthalpy.
Effective Conductivity

$$k_{eff} = \gamma k_{feff} + (1 - \gamma) k_s \tag{7}$$

Where γ is the porosity, when γ=1 there is only fluid, k_{feff} the fluid effective conductivity and k_s the solid conductivity. The fluid effective thermal conductivity is given by

$$k_{feff} = k_f + k_t \tag{8}$$

Where k_f is the fluid conductivity and k_t the turbulent conductivity given by
Turbulent Conductivity

$$k_t = \frac{C_p \mu_t}{\mathrm{Pr}_t} \tag{9}$$

Where, C_p is the specific heat capacity and Pr_t the turbulent Prandtl number while the enthalpy h is given by the equation

$$h = \int_{T_0}^{T} C_p dT \tag{10}$$

The calculation of the energy equation source term is important because incorporates the effect of radiation in the energy balance and it is taken from the solution of the radiative transport equation. When the velocity takes null value, as it happens in solid materials, the above equation is decreased in the equation of conductivity for heat transfer.

$$\rho \frac{\partial T}{\partial t} + k_s \frac{\partial^2 T}{\partial x_i^2} + S_h = 0 \tag{11}$$

4.5. Turbulent model

The flow in both internal and external air is turbulent. The effect of turbulence is implemented via the high Re k-ω model of Wilcox [21](Wilcox, D. C., 1998).
Turbulent kinetic energy, k, transport equation is given by

$$\rho \frac{\partial k}{\partial t} + \rho U_j \frac{\partial k}{\partial x_j} = \tau_{ij} \frac{\partial U_i}{\partial x_j} - \beta^* \rho k \omega + \frac{\partial}{\partial x_j}\left[\left(\mu + \mu_t \sigma^* \right) \frac{\partial k}{\partial x_j} \right] \tag{12}$$

Where, ω is the specific dissipation rate, for which the transport equation is

$$\rho \frac{\partial \omega}{\partial t} + \rho U_j \frac{\partial \omega}{\partial x_j} = \alpha \frac{\omega}{k} \tau_{ij} \frac{\partial U_i}{\partial x_j} - \beta \rho \omega^2 + \frac{\partial}{\partial x_j}\left[\left(\mu + \mu_\tau \sigma \right) \frac{\partial \omega}{\partial x_j} \right] \tag{13}$$

with $\omega = \frac{\varepsilon}{\beta^* k}$, $\mu_\tau = \frac{k\rho}{\omega}$, α=5/9, β=3/40, β*=9/100, σ=1/2 and σ*=1/2, where ε is the turbulence dissipation rate.

4.6. Radiation model

In order to simulate the effect of solar incident radiation on the trailing plants, the shelter and the test cell walls, the Discrete Ordinates (DO) model is used. In this model it is assumed that radiation energy is 'convected' through the medium at its own speed simultaneously in all directions. The DO model allows the solution of radiation at semi-transparent walls. It can be used to non-gray radiation using a gray-band model. So it is adequate for use with participating media with a spectral absorption coefficient α_λ that varies in a stepwise fashion across spectral bands. The DO radiation model solves the Radiative Transfer Equation (RTE) for a finite number of discrete solid angles, each associated with a vector direction $\vec{s}$ fixed in the global Cartesian system (x,y,z). It transforms the RTE equation into a transport equation for radiation intensity in the spatial coordinates (x,y,z). The DO model solves for as many transport equations as there are directions $\vec{s}$ (Raithby, G. D. & Chui, E. H., 1990; Chui, E. H. & Raithby, G. D., 1993). The RTE for spectral intensity $I_\lambda(\vec{r},\vec{s})$ turns to

$$\nabla\left(I_\lambda(\vec{r},\vec{s})\vec{s}\right) + \left(a_\lambda + \sigma_s\right) I_\lambda(\vec{r},\vec{s}) = a_\lambda n^2 I_{b\lambda}(\vec{r}) + \frac{\sigma_s}{4\pi} \int_0^{4\pi} I_\lambda(\vec{r},\vec{s}') \Phi(\vec{s}\cdot\vec{s}) d\Omega \tag{14}$$

In this equation the refractive index, the scattering coefficient and phase function are assumed independent of wavelength. The phase function Φ, is considered isotropic. The angular space 4π at any spatial location is discritized into $N_\theta x N_\varphi$ solid angles of extent ω_i, called control angles. The angles θ and φ are the polar and azimuthal angles, and are measured with respect to the global Cartesian system (x,y,z). In our case a 3x3 pixilation is used. Although in this equation the refraction index is taken constant, in the calculation of black body emission as well as in the calculation of boundary conditions imposed by semi-transparent walls the band length depended values of refractive index are used. This angular discretization provides us with a moderate computational cost but it may introduce discretization errors at boundaries when the solid angles are bisected by them (Raithby, G. D., 1999). Solving a problem with a fine angular discretization is very CPU-intensive. The RTE equation is integrated over each wavelength. Then the total intensity $I(\vec{r},\vec{s})$ in each direction $\vec{s}$ at position $\vec{r}$ is computed using

$$I(\vec{r},\vec{s}) = \sum_{\kappa} I_{\lambda_\kappa}(\vec{r},\vec{s})\Delta\lambda_\kappa \tag{15}$$

Where, the summation is over the wavelength bands. The RTE equation is coupled with the energy equation through a volumetric source term given by the following equation (Kim, S. H. & Huh, K. Y., 2000):

$$S_h = -\frac{\partial q_{r_i}}{\partial x_i} = a_\lambda\left(4\pi I_{b\lambda}(\vec{r}) - \int_{4\pi} I(\vec{r},\vec{s})\,d\Omega\right) \tag{16}$$

The spectral absorption coefficient, α_λ is computed from the absortpivity, α, according to the media thickness, d:

$$\alpha_\lambda = \frac{1}{d}\ln\left(\frac{1}{1-\alpha}\right) \tag{17}$$

5. Numerical model

The problem is simulated through 2D transport equations for mass, momentum, turbulence, energy and spectral radiation. Those transport equations (1, 2, 6, 12, 13 and 14) are solved numerically using the finite volume method.

5.1 Grid geometry

For the simulation is used a structured collocated grid consisted of 18864 cells as shown in the following Fig.3. The internal air field is consisted of 12400 cells. The external air field is consisted of 3744 cells. The plants are considered porous media consisted of 432 cells. The transport equations are also solved inside the solid walls which are discretized to 4 series and inside the shelter which is discretized to 3 series of cells resulting to 2288 cells in total.

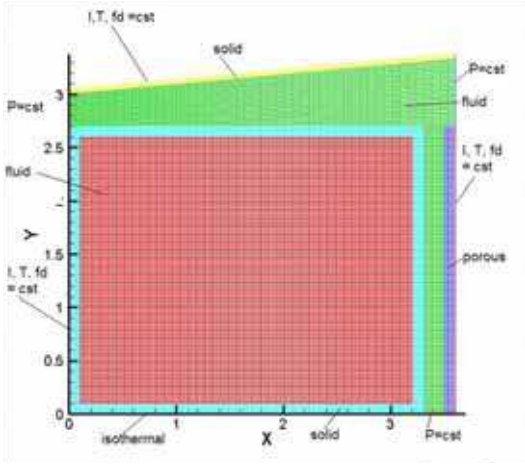

Fig. 3. Grid and Boundary conditions

5.2 Boundary conditions

The floor was assumed as a constant temperature wall, opaque which emits diffusively at an emissivity of ε = 0.92/0.72 depended on the wavelength band. For all the examined cases the floor temperature is set to T=293 K which is a simplifying approach.

In the North wall a mixed heat transfer boundary condition (combination of radiation and convection) is applied at the external boundary of the solid region. As far it concerns the radiation it is considered semi-transparent material where all the incident radiation is diffusive. A semi-transparent boundary condition implies that the incident radiation is reflected or transmitted by the surface. For that, the absorption coefficient of the adjacent solid zone is taken high enough to ensure that the whole transmitted radiation will be absorbed. This way the whole wall becomes opaque and the incident radiation is either reflected from the surface either absorbed, increasing the wall temperature. The heat transfer coefficient is taken h=7.1 W/mK.

The same boundary condition is imposed at the external surface of the shelter, where the heat transfer coefficient is set h=20 W/mK, and at the external south surface of the plants, where the heat transfer coefficient is set h=7.1 W/mK too. In the plants external surface the wall non-slip condition is substituted by a zero shear stress boundary condition. In this case the absorption coefficient of the adjacent porous material does not absorb all the transmitted incident radiation, but only a part of it.

All the internal walls are considered to be semi-transparent surfaces where the solid and fluid zones are coupled. This way the values of the variables are transferred from the one medium to the other. The trailing plants are considered as porous media with viscous resistance coefficient $\left(1/a\right) = 27380\,[m^{-2}]$, where a is the permeability and inertial resistance coefficient C_2= 1.534 [m^{-1}]. The porous material is coupled with the external boundary surface and the adjacent fluid. The equations of energy and radiations are also solved in all the solid and porous areas of the computational field. The flow both in the internal and the external fields is considered turbulent since the Ra number for the internal flow is 1.5×10^{10} and the Re number for the external flow is more than 1.9×10^{4}.

All the openings from where external air can enter or leave the computational field (right down opening between test cell and plants, right up opening between shelter and plants and left up opening between test cell and shelter) are considered as boundaries with constant pressure equal with atmospheric. The flow direction is determined by the whole field behavior as it is developed due to temperatures and the arising buoyancy forces. The air temperature in openings is set equal to the external air temperature.

When radiation reflected and transmitted from a specular semi-transparent surface, as it happens partly in our case, its direction is altered. The reflected radiation is given by

$$I_{W,a}\left(\vec{s}_r\right) = r_a\left(\vec{s}\right) I_{W,a}\left(\vec{s}\right) + \tau_b\left(\vec{s}'\right) I_{W,b}\left(\vec{s}_b\right) \tag{18}$$

Where, $I_{W,a}$ radiation intensity in the medium a, which is the air in our case, $I_{W,b}$ radiation intensity in the medium b, which is the solid, $\vec{s}$, direction of the incident radiation (from a to b), $\vec{s}_r$ direction of the reflected radiation, $\vec{s}'$, direction of the radiation incident to the surface from the solid side (from b to a), r_a , the interface air reflectivity and τ_b , the interface solid transmissivity. The radiation transmitted from the semi-transparent wall towards the solid is given by

$$I_{W,b}\left(\vec{s}_t\right) = r_b\left(\vec{s}'\right) I_{W,b}\left(\vec{s}\right) + \tau_a\left(\vec{s}'\right) I_{W,a}\left(\vec{s}_b\right) \tag{19}$$

Where, $\vec{s}$ is the direction of the refracted radiation inside the solid, r_b, the interface solid reflectivity and τ_a, the interface air transmissivity. The radiation directions are given by

$$\vec{s}' = \vec{s}_t - 2\left(\vec{s}\cdot\vec{n}\right)\vec{n} \tag{20}$$

Where, $\vec{n}$ is the normal to boundary unit vector, and

$$\vec{s}_r' = \vec{s} - 2\left(\vec{s}\cdot\vec{n}\right)\vec{n} \tag{21}$$

The interfaces' reflectivities and transmissivities are given by

$$r_a\left(\vec{s}\right) = \frac{1}{2}\left(\frac{n_a\cos\theta_b - n_b\cos\theta_a}{n_a\cos\theta_b + n_b\cos\theta_a}\right)^2 + \frac{1}{2}\left(\frac{n_a\cos\theta_a - n_b\cos\theta_b}{n_a\cos\theta_a + n_b\cos\theta_b}\right)^2 \tag{22}$$

$$\tau_b\left(\vec{s}'\right) = 1 - r_a\left(\vec{s}\right) \tag{23}$$

finally $r_b = r_a$ and $\tau_a = \tau_b$.

Where, n_a is the air refractive index, n_b the solid refractive index, θ_a the angle between the normal to the surface and the incident radiation direction $\vec{s}$ and θ_b, the angle between the normal to the surface and the refracted radiation direction inside the solid $\vec{s}_t$. It is obvious that in the case of unsteady calculations, those parameters should be calculated in every time step in each surface since the angle of incident radiation varies through the whole day.

$$\theta_b = \arcsin\left(\frac{n_a}{n_b}\sin\theta_a\right) \tag{24}$$

It should be noted that the above holds for $n_a < n_b$. The angle θ_a is given by (Duffie, J. A. & Beckman, W. A., 1991)

$$\cos\theta_a = \left(A - B\right)\sin\delta + \left[C\sin\omega + \left(D + E\right)\cos\omega\right]\cos\delta \tag{25}$$

$A = \sin\phi\cos\beta$, $B = \cos\phi\sin\beta\cos\gamma$, $C = \sin\beta\sin\gamma$, $D = \cos\phi\cos\beta$, $E = \sin\phi\sin\beta\cos\gamma$

Where, φ is the latitude (φ= 39º 38 in our case), δ is the declination, β is the surface slope, γ is the surface azimuth angle and ω is the hour angle. For the vertical south wall of plants it is

taken β=90° and γ=0°. For the shelter external surface it is taken β=5° and γ=180°. The angles δ and ω are given by

$$\delta = 23.45\sin\left(\frac{360(284+n)}{365}\right) \tag{26}$$

$$\omega = \left[(t_s + t) - 12\right]15 \tag{27}$$

Where, n is the day of the year, t_s and is the sunrise time.

5.3 Numerical details

The SIMPLEC (Patankar, S. V., 1980) algorithm is used for pressure-velocity coupling, yielding an elliptic differential equation in order to formulate the mass conservation equation. The discretisation of the convective terms in the Reynolds averaged transport equations is materialized by the QUICK scheme for the momentum equations, a second order upwind scheme (SOU) for the turbulence and radiation transport equations and by a third order MUSCL for the energy conservation equation. For the diffusive terms a central difference scheme is adopted. The convergence criterion was set to 10^{-4} for the continuity, momentum and turbulence equations while for energy the criterion was 10^{-8} and for radiation 10^{-6}. For the radiation model two wavelength bands are considered corresponding to solar spectrum (λ=0 -1.1 μm) and to thermal band (λ=1.1 – 100 μm).

6. Reference case

In order to validate the numerical model our study began with the simulation of a summer day for which experimental data about incident solar radiation, ambient temperature and temperatures developed inside the test cell infrastructure exists. For the validation it was chosen the simulation of 22nd of August of 2006 (Tzachanis A.D., 2008).

6.1 Experimental configuration

The experiments, used for validation, were carried out at the South-orientated façade of the test cell during a hot summer period (July to September) in Larissa, a Greek city with a climate characterized by long hot days in the summer. The measured data are presented in paper (Tzachanis, A.D, 2008). With a set of pyranometers with and with out shading rings were measured the diffuse irradiation, the beam irradiation and the global irradiation in a horizontal plane, as well as the global irradiation and the ground reflected irradiation in a vertical plane. The temperatures were also measured in the ambient, sunlit wall, shadowed wall and in the gap between the plants and the south wall by NiCr thermocouples.

6.2 Numerical configuration

The daily variations of incident irradiations and ambient temperature were approached with polynomials, in order to be used as boundary conditions in the simulation. The corresponding polynomials are given following

For the irradiation in vertical plane

$$I_v = -6.7 - 7.48x10^{-3}time + 6.21x10^{-6}time^2 - 2.38x10^{-10}time^3 + 2.33x10^{-15}time^4 \tag{28}$$

For the irradiation in horizontal plane

$$I_h = -1.74 + 6.28x10^{-3}\,time + 4.57x10^{-6}\,time^2 - 1.83x10^{-10}\,time^3 + 1.79x10^{-15}\,time^4 \quad (29)$$

For the ambient temperature

$$T_{amb} = 2.13 - 5.87x10^{-4}\,time + 2.29x10^{-7}\,time^2 - 1.72x10^{-11}\,time^3 + 5.97x10^{-16}\,time^4 - 1x10^{-20}\,time^5 + 6.43x10^{-26}\,time^6 \quad (30)$$

Where, *time* is the time since sunrise in secs. In both plane the percentage of diffuse irradiation f_d was 30%. Since there are not experimental measurements, it was supposed that the north wall received the half irradiation than the plants' vertical surface and that all of this irradiation was diffusive, f_d=1. In the 22nd of August in Larissa (φ=39.38°, L=22.25°) the solar sunrise time is 6h 39′ 36′′. Our simulation will begin from 6h 00′ 00′′ in the morning giving the opportunity to the flow field to reach a steady state condition, before the boundary conditions begin to alternate. The whole period of simulation is the total solar day from 6 h 00′ 00′′ up to 19h 20′ 00′′, a few minutes after the sunset. The time step is dτ=1 sec. The simulation results are saved every 60 secs.

6.3 Model validation

The numerical model was validated against the experimental measurements. Three temperatures were compared. The temperature developed in the gap between the plants and the shaded south wall, the temperature developed on the shaded south wall and the temperature developed on the sunlit surface. As simulated temperatures are considered the average temperatures: a) on a line across the gap in the elevation of 1.35 m for the gap temperature, b) on the surface of the south wall, for the shaded wall temperature, and c) in the surface on the sunlit shelter for the sunlit temperature. In the following figures 4, 5 and 6 the measured and simulated temperatures temporal profiles are given. The simulated temperatures are also compared with the temperatures calculated by steady-state simulations realized for the hours 8:00, 10:00, 12:00, 14:00, 16:00 and 18:00.

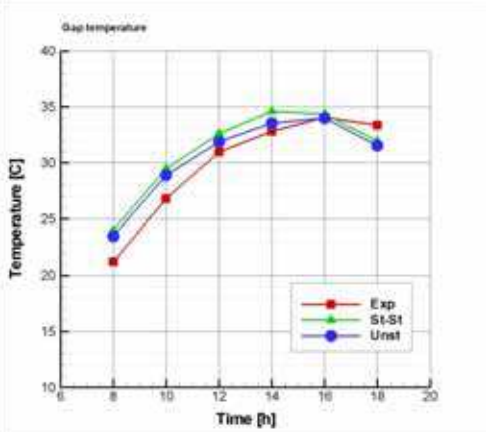

Fig. 4. Temporal profile of gap temperature

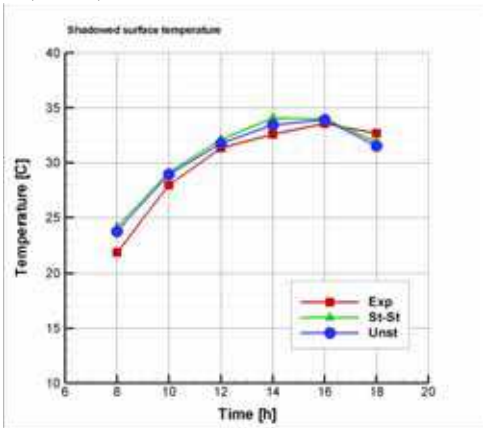

Fig. 5. Temporal profile of shadowed surface temperature

As far it concerns the gap and shaded surface temperatures we observe a fairly good approach with the unsteady simulation giving better results from the steady-state

simulation since it takes into account the phenomenon of thermal storage. The average deviation of unsteady simulation to the measured temperatures is of the order of 10%. Almost all the day the real temperatures are lower than the predicted. This is due to the fact that transpiration and the subsequent temperature decrease is not incorporated in the proposed model.

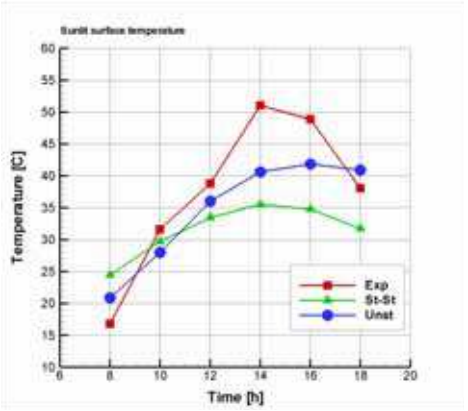

Fig. 6. Sunlit surface temporal temperature profile

As far it concerns the sunlit surface temperature profile we observe significantly more important improvement of temperature predictions passing from steady-state to unsteady radiation, in the order of 30% but the predicted values are still away from the measured especially for the hours between 14:00 and 16:00. As it has been pointed in the boundary conditions section a mixed boundary condition, taking account both convection and radiation, has been implemented to the shelter outer surface. Since the field around the shelter outer surface is not solved in this simulation a constant convection coefficient was adopted during all the day. It is likely at the afternoon hours the external wind speed to be enough low, so as to it led to a convection coefficient much lower than assumed. This could explain the deviation between measured and simulated temperatures during those hours.
In general the comparison is considered successful and the model is considered to simulate with fairly accuracy the transport phenomena takes part in the studied field. In following figures the most important flow and heat parameters in 6 characteristic hours are given in terms of iso-contours, streamlines and profiles. In fig.7 the temperature iso-contours inside the test cell are given for the hours 8:00, 10:00, 12:00, 14:00, 16:00 and 18:00.

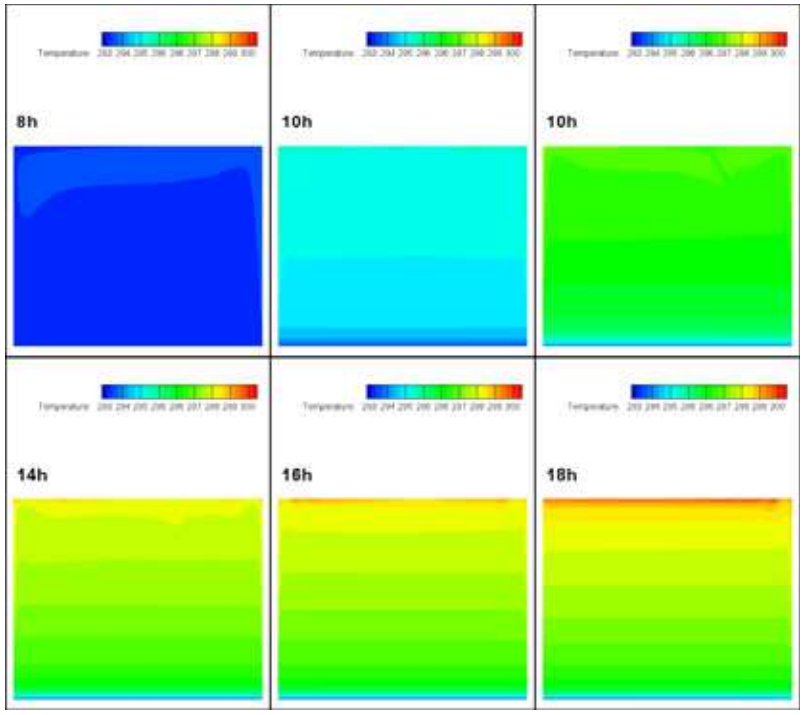

Fig. 7. Temperature iso-contours

During the day the temperature does not exceed the 27 °C, with the higher temperatures appearing at 18:00 h in the afternoon in the top of the cell. Although the north wall receives only diffusive radiation with the half intensity than the south the plants existence provide enough shadow to keep the south wall temperature low enough to cancel the appearance of any temperature gradient. The temperature in the floor remains 20 °C because it was selected to adopt the particular simplifying admission of isothermal boundary condition. In Fig.8 the temperature iso-contours around the test cell and between the cell and the shading devices are presented. In the external studied field the temperature can be as high as 36 °C, due to increased external air temperature and the heating through conduction, convection and irradiation. The higher temperature is observed in the 16:00 in the afternoon.

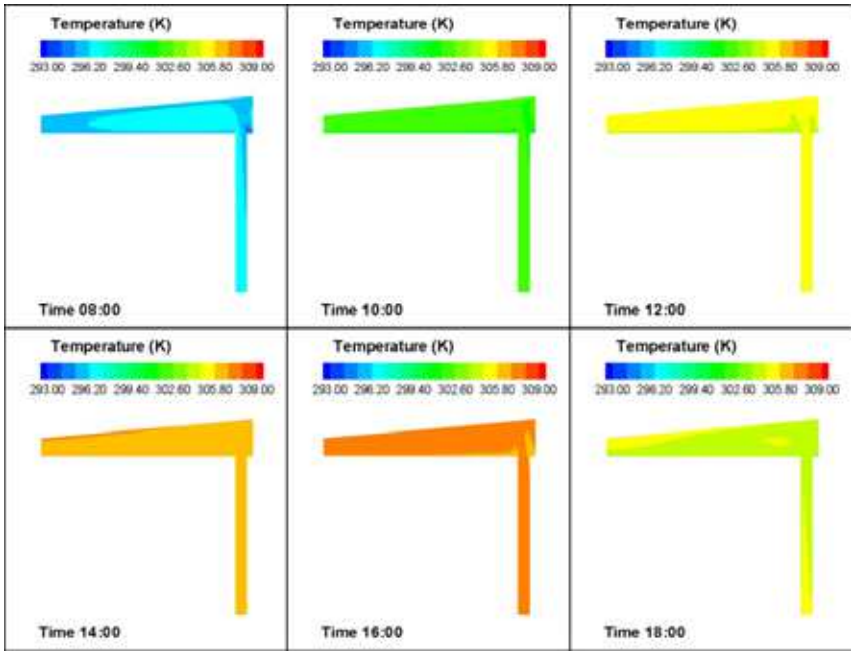

Fig. 8. Temperature iso-contours around the test cell

Finally in the figures 9 and 10 the temperature profiles along the x and y symmetry axes of the test cell are presented. The luck of any horizontal temperature gradient is verified. In the horizontal symmetry axis the temperature increase until 14:00 and then remains almost constant. The same behavior is observed along the vertical axis where the higher gradient appears during the afternoon.

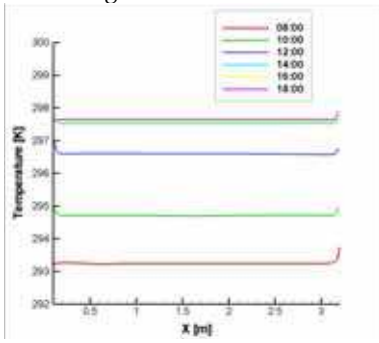

Fig. 9. Horizontal symmetry axis temperature profile

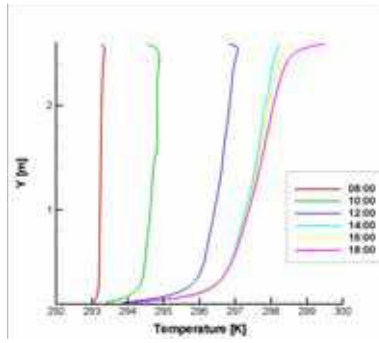

Fig. 10. Vertical symmetry axis temperature profile

In the figures 11 and 12 the streamlines and the isobaric contours are presented for the internal and the external field and the same hours.

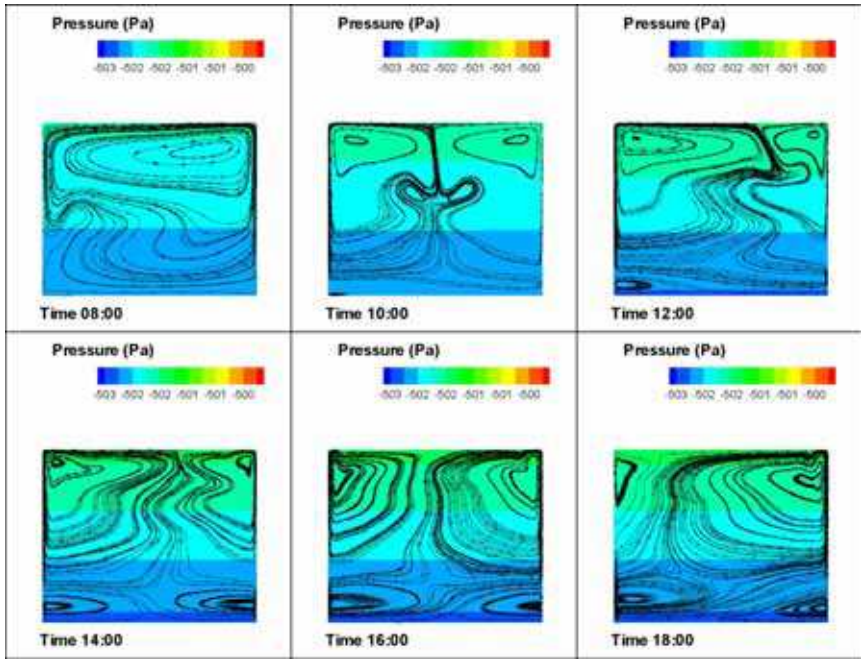

Fig. 11. Streamlines and isobaric contours inside the test cell

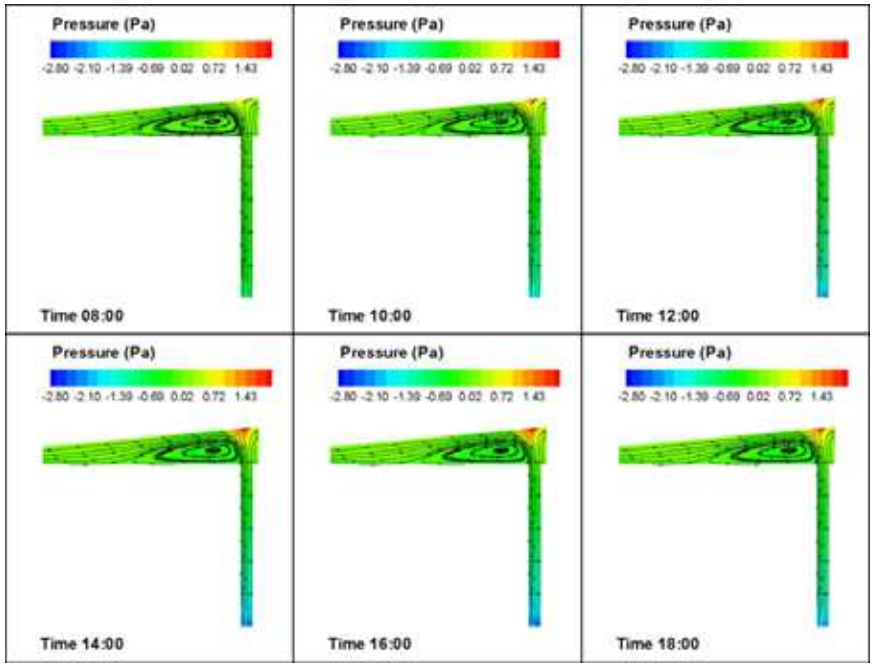

Fig. 12. Streamlines and isobaric contours outside the test cell